

Electronic Supplementary Information

Fundamentals of Ion Motion at Atmospheric Pressure and Simulation Environment

The simulation of gaseous ion trajectories has been used extensively in the development of ion optics for MS, IMS, electron microscopes (EM), and focused ion beam (FIB) systems. In the case of systems operating in high-vacuum (EM and FIB) the simulation environment is often simplified and assumed to be collision-free and ion motion is influenced purely by electric and magnetic fields; however, IMS and many MS systems operate in a pressure regime in which collisions cannot be neglected. SIMION 8.0 includes two collision models (HS1 and SDS) that can be incorporated for the treatment of these collisions. HS1 employs hard-sphere collision kinetics to compute the resulting ion trajectory change for ion-molecule collisions individually¹. This approach is not computationally feasible at atmospheric pressures as the mean free path in air at 25 °C is approximately 67 nm². Rather than treating individual collisions, the SDS algorithm uses a combined approach of diffusion and ion mobility to simulate ion motion in electric fields.

The motion of ions at atmospheric pressure is heavily influenced by the diffusion of ions in the medium, as well as by external forces exerted on the ions (electric fields, bulk gas flow, etc.). Diffusion can be expressed as:

$$J = D\nabla_n \quad \text{Eq. 1}$$

where J , D , and ∇_n are the number of ions passing through an area normal to the gas flow, a proportionality constant, and the concentration gradient, respectively³. In the SIMION-SDS algorithm, diffusion is simulated by imposing a random ion jump onto the ion trajectory. The radius of the jump is determined by an interpolation between collision statistics tables (selected based on the mass ratio of the ion to a background gas molecule) and scaled appropriately based on an expected number of collisions in the simulation time step⁴.

When subjected to an electric field (E), the velocity of an ion in a gas with no bulk flow is determined by its mobility (K) in the buffer gas³.

$$v = KE \quad \text{Eq. 2}$$

K is determined experimentally and is directly proportional to D and the charge (e) on the ion and inversely proportional to temperature (T) multiplied by the Boltzmann constant (k)³.

$$K = \frac{eD}{kT} \quad \text{Eq. 3}$$

This is known as the Nernst-Townsend relation and holds for the cases in which ions are thermalized. The mobility can further be expressed as⁵:

$$K = \frac{3e}{16N} \left(\frac{2\pi}{\mu kT} \right)^{1/2} \left(\frac{1}{Q_D} \right) \quad \text{Eq. 4}$$

Where N is the density of the neutral molecules, μ is the reduced mass of the collision pair, and Q_D is the collisional cross section. Due to the range of working conditions used in IMS instruments, the mobility of an ion is often reported as the reduced mobility (K_0) which is corrected for 273 K and a pressure (P) of 760 Torr:

$$K_0 = K \left(\frac{273}{T} \right) \left(\frac{P}{760} \right) \quad \text{Eq. 5}$$

At each time step within a SIMION-SDS simulation, the velocity of an ion is subjected to the effects of gas flow and the applied electric field, in the form of mobility (Eq. 2). A simulated diffusion in the form of a random jump is superimposed on this motion to determine the location of the ion during the start of the next time-step. A more detailed discussion of the SDS algorithm is provided in the literature and in the SIMION 8.0 documentation⁴. The SDS algorithm is capable of either using a defined mobility for each ion, or in the cases in which this data is not available, known information (particle diameters, masses, etc.) is used to estimate a value for ion mobility. Spatial variations in gas flow, pressure, and temperature may also be incorporated into the SDS algorithm to more accurately model conditions in which these parameters are known. Effects due to space charge can also be included in the modeling; however, ions must be flown as a group when incorporating space charge effects into an SDS simulation. For all simulations performed in this work, bulk gas flow was assumed to be zero and space charge was not considered in order to decrease computational time.

Simulation of 2D ion distribution at deposition surface

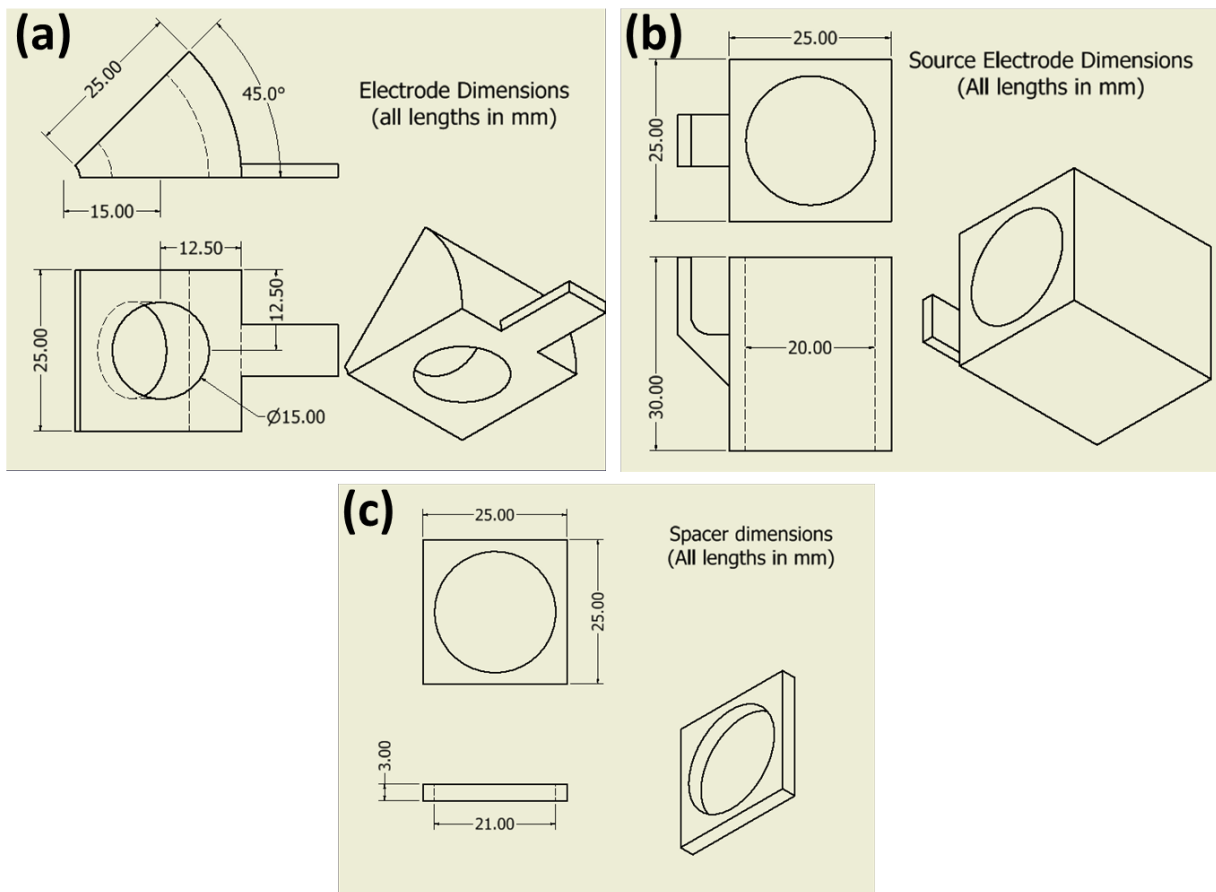
The potential arrays (PA) used in the simulation of both the 2D ion distribution at the deposition surface (Figure 2c and 2d) and the separation of tetraalkylammonium (TAA) cations (figure 4b) were generated from .stl format using the “Convert STL -> PA” option in the SIMION 8.0 SL Tools. A 0.2 mm/grid unit resolution was selected to mimic the 0.2 mm layer height resolution at which the electrodes were printed and the solid strategy was set as “solid points under surface normal”.

For the simulation of the mesh used for ion injection in the TAA cation separation, the mesh was modeled as a plane with a thickness equal to the grid cell size (0.2 mm). Because SIMION treats a plane of 1 grid unit as a 100% transmission ideal grid, this means that the simulated mesh passes ions at all points. This simplification was made to decrease computational time in the simulation as a smaller unit cell size (<0.2mm/grid unit) is required to model the woven mesh in its true form which would result in a much larger PA space.

In the case of the simulated 2D ion distribution at the deposition surface, ions were initiated with a 3D Gaussian distribution (σ_x , σ_y , and $\sigma_z = 5$ mm) in the center of the source electrode with a single time of birth (TOB). The contour plots of simulated ion distribution (Figure 2c and 2d) were generated using a histogram bin width of 0.05 mm x 0.05 mm.

The simulation of ion separation was performed by initiating all ions with a uniform cylindrical distribution within the area between the two mesh electrodes. At the start of the simulation time step, the injection voltage was set to the high value used for injection (2530 V) for 50 ms, after which it was set to the low value (2480 V) for the remainder of the simulation time period. This approach is not meant to accurately model the ion distribution between the mesh electrodes during the injection, but is used to simplify the simulation so that arrival times of ions at the detector (a mass spectrometer in this case) can be approximated to determine if simulation values agree with experimental data.

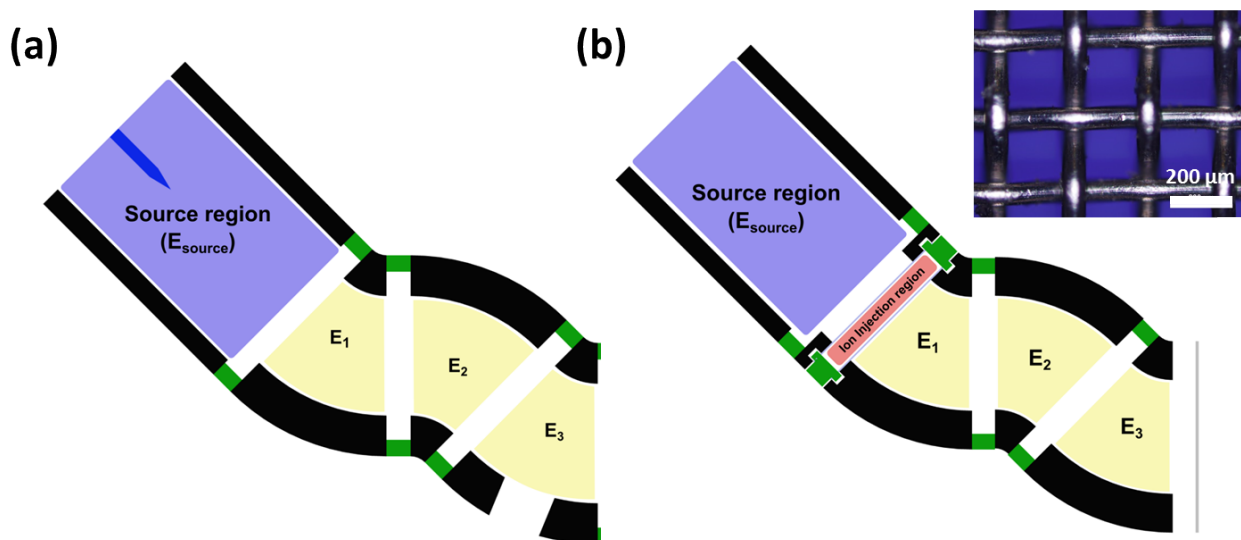
Electrode and spacer dimensions



S1: Dimensional drawings of turning electrodes (a), source electrode (b), and spacers (c).

Ion injection assembly

Controlled injection of ions into the turning electrodes was accomplished by modifying the electrode system shown in figure 1 to include a region separated by two wire meshes (S2b, ion injection region). The mesh closest to the source electrode was held at a low value of 2480 V which prevented the transmission of ions into the curved electrodes. Ions were injected into the curved electrode region by pulsing this voltage to a value of 2530 V for 50 ms.

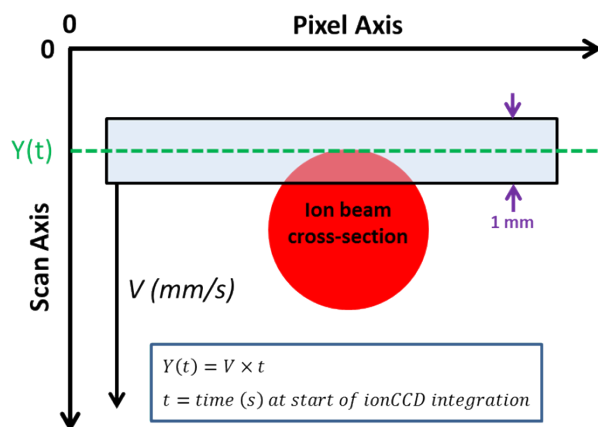


S2: Illustrations of electrode assemblies used for ion/molecule reactions (a) and ion separation experiments (b). Different regions of the electrode system are highlighted and an optical image of the stainless steel mesh used in the ion injection region is shown inset (b).

Profiling of beam using ionCCD

The ion beam exiting the electrode assembly was profiled by mounting the ionCCD detector on a moving stage and scanning the detector slit across the exit of the last electrode at a fixed rate of 0.100 mm/s. A diagram of this process is shown in S3. A potential of 10 V was applied to the ionCCD housing during the signal acquisition. This potential served to increase the electric field strength between the floated detector array and the aluminum enclosure (0.711 mm gap between housing and detector array), thus drawing ions to the detector surface which results in a stronger signal.

The 2D intensity plots were reconstructed from the data by a Matlab script which uses the integration time (100 ms in all experiments) along with the velocity of the moving stage to calculate position along the scan axis ($Y(t)$) for each detection cycle of the ionCCD.



S3: Diagram illustrating how ionCCD data was captured and the data assembled into a 2D plot of ion intensity from individual integration time steps. The detector slit is indicated by the blue transparent box.

The elongation seen in the reconstructed intensity plots (figure 2a and 2b) when compared to the simulated 2D ion distribution at the electrode exit is likely a result of both the gap between the stainless steel housing and the detector surface as well as the width of the pixel array (1 mm). The elongation in the pixel axis is likely the result of ions diffusing outward after entering the gap between the housing and the detector surface. The 10 V potential serves to negate this effect slightly, but application of larger potentials poses the risk of damaging the detector electronics. The width of the pixels most certainly contributes to an elongation in the reconstructed signal intensity along the scan axis. For example, at a scan rate of 0.100 mm/s the detector slit moves approximately 0.100 mm during an integration time step which is only 10% of the pixel width. This means that the position assigned to each integration time step along the scan axis also includes the entirety of ions exiting the electrode $\pm 500 \mu\text{m}$ from the assigned position ($Y(t)$).

Ion transmission efficiency

The transmission of ions through the device was examined experimentally by spraying a $10 \mu\text{M}$ mixture each of tetrapropyl-, tetrabutyl-, tetrahexyl-, and tetradodecylammonium bromide in ACN through a pulled nanoESI emitter ($5 \mu\text{m}$ tip) into the source region (E_{source}) of the device shown in S2a. Ion current impinging on an Al coated glass slide (I_{surface}) positioned 1 mm from the opening of E_3 was measured using a Keithley 6487 picoammeter. The total spray current (I_{spray}) was determined by monitoring the voltage drop across a $4.7 \text{ M}\Omega$ resistor in connected in series between the spray tip and high voltage source. Unless otherwise noted, for these experiments the spray tip was inserted 1 cm into E_{source} and

potentials applied to each electrode were identical to those given in figure 2a and 2c. A summary of the results of these experiments is shown in table S4 below.

Table S4: Efficiencies of ion transfer from spray tip to deposition surface under typical operating conditions. Potentials applied to E_{source} , E_1 , E_2 , and E_3 are identical to figure 2a and 2c. Spray voltage is given as the difference of potential applied to emitter and potential applied to E_{source} .

Spray voltage (kV)	I_{source}	I_{surface}	Transmission efficiency
0.750	3.52	0.28	7.8%
1.00	19.65	0.50	2.5%
1.25	37.99	0.67	1.8%
1.50	56.56	0.75	1.3%
1.65	67.70	0.87	1.3%

It is clear from these numbers that with an increased spray voltage there is significant drop in transmission efficiency. This is likely due to ions being driven into the walls of E_{source} by the increased electric field strength between the spray tip and the walls of E_{source} as well as the increasingly dispersive nature of the spray plume at higher potentials.

It is possible to increase transmission efficiency by iteratively tuning the potentials on each electrode as well as the spray tip. With the tip position maintained as in S4 (inserted 1 cm into E_{source}) it was possible to transmit 11% of an 11.10 nA current through the device. To achieve this, potentials of 3.89 kV, 3.00 kV, 2.64 kV, 1.89 kV, and 1.37 kV were applied to the spray tip, E_{source} , E_1 , E_2 , and E_3 , respectively. While the ion distribution at the surface was not mapped under these conditions, simulations show a significant increase in spot size at the detection surface. By further adjustment of potentials and inserting the nanoESI emitter further into E_{source} (approximately 10 mm distant from the opening of E_1) a 55% transmission of a 4.01 nA spray current was achieved. Potentials applied to the spray tip, E_{source} , E_1 , E_2 , and E_3 were 3.65 kV, 2.50 kV, 1.76 kV, and 1.27 kV, respectively.

Simulations were used as the primary tool in determining where ion losses might occur within the devices. Under typical operating conditions as shown in figure 2a and 2c, a simulation was performed in which the ions were originated uniformly within a cylindrical volume extending from the tip of a nanoESI emitter (inserted 1 cm into E_{source} as is visible in figure 1c) to the exit of the E_{source} . From this simulation an “acceptance volume” (defined as the volume within the source capable of transmitting ions to the deposition surface) was determined. The transmission efficiency was also calculated from the simulated trajectories of 4×10^4 ions (10^4 of tetrapropyl-, tetrabutyl-, tetrahexyl-, and tetradodecylammonium cations) distributed uniformly within the cylindrical volume. The resulting acceptance volume is shown in figure S5 below along with a plot of origin locations of all ions within acceptance volume. Electrode points and resulting deposition spot are shown as well.

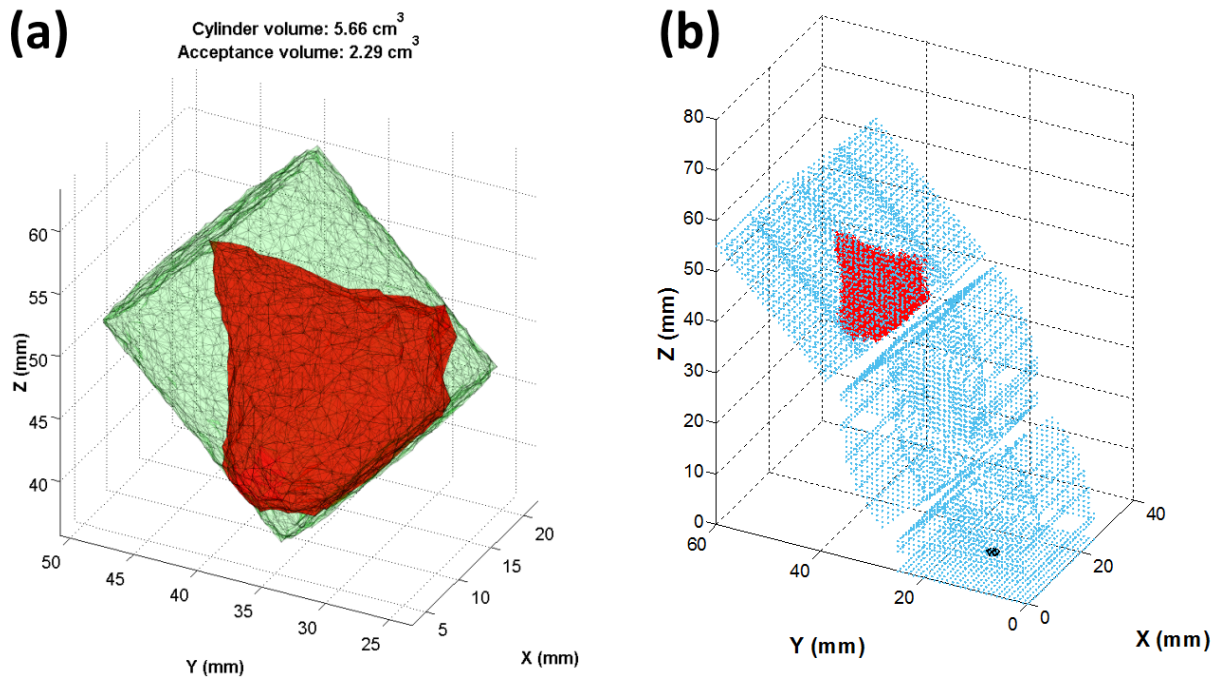


Figure S5: Volume encompassing ion origin locations represented by green mesh, and acceptance volume represented by red mesh (a); 3D scatter plot showing origin location of ions within acceptance volume (red points), electrode points (blue), and resulting deposition spot (black)(b). Potentials applied to emitter and electrodes are identical to figure 2a and 2c.

From the calculated volumes of the ion origins and resulting acceptance volume a maximum transfer efficiency from ions originating only within E_{source} can be calculated as 40.5%. This number assumes that ion generation occurs only within E_{source} which is not representative of the dynamic nature of spray ionization in which gas phase ions may be released from droplets projected beyond the confines of E_{source} . A qualitative examination of simulated ion trajectories suggests that the majority of losses occurs to the walls of E_{source} with minor losses to the walls of E_1 . Ion losses within electrodes E_1 - E_3 are assumed to be minimal and the transmission efficiency of more than 50% achieved by positioning the spray tip within 10 mm of the entrance of E_1 support this reasoning. It is expected that with further optimization of the size and shape of electrodes, transmission efficiencies may be increased significantly.

1. D. J. Manura and D. A. Dah., *SIMION 8.0 User Manual*, Scientific Instrument Services, 2008.
2. S. G. Jennings, *Journal of Aerosol Science*, 1988, 19, 159-166.
3. G. A. Eiceman, Z. Karpas and H. H. Hill, *Ion Mobility Spectrometry, Third Edition*, Taylor and Francis, Hoboken, 2013.
4. A. D. Appelhans and D. A. Dahl, *International Journal of Mass Spectrometry*, 2005, 244, 1-14.
5. E. A. Mason and E. W. McDaniel, in *Transport Properties of Ions in Gases*, Wiley-VCH Verlag GmbH & Co. KGaA, 2005, pp. 137-193.